



Alpha-Tubulin Acetylation in *Trypanosoma cruzi*: A Dynamic Instability of Microtubules Is Required for Replication and Cell Cycle Progression

OPEN ACCESS

Edited by:

Sabrina Absalon,
Indiana University, United States

Reviewed by:

Veronica Jimenez,
California State University, Fullerton,
United States
Carlos A. Buscaglia,
Consejo Nacional de Investigaciones
Científicas y Técnicas (CONICET) y la
Universidad Nacional de General San
Martín, Argentina

*Correspondence:

Esteban Serra
serra@ibr-conicet.gov.ar
Maria Cristina M. Motta
motta@biof.ufrj.br

†Present address:

Mara Emilia Carloni,
Yersinia Research Unit, Microbiology
Department, Institut Pasteur,
Paris, France

Specialty section:

This article was submitted to
Parasite and Host,
a section of the journal
Frontiers in Cellular and Infection
Microbiology

Received: 15 December 2020

Accepted: 08 February 2021

Published: 11 March 2021

Citation:

Alonso VL, Carloni ME, Gonçalves CS,
Martinez Peralta G, Chesta ME,
Pezza A, Tavernelli LE, Motta MCM
and Serra E (2021) Alpha-Tubulin
Acetylation in *Trypanosoma cruzi*: A
Dynamic Instability of Microtubules Is
Required for Replication and
Cell Cycle Progression.
Front. Cell. Infect. Microbiol. 11:642271.
doi: 10.3389/fcimb.2021.642271

Victoria Lucia Alonso^{1,2}, Mara Emilia Carloni^{2†}, Camila Silva Gonçalves^{3,4},
Gonzalo Martinez Peralta^{1,2}, Maria Eugenia Chesta⁵, Alejandro Pezza¹,
Luis Emilio Tavernelli¹, Maria Cristina M. Motta^{3,4*} and Esteban Serra^{1,2*}

¹ Laboratorio de Biología y Bioquímica de *Trypanosoma cruzi*, Instituto de Biología Molecular y Celular de Rosario (IBR), Consejo Nacional de Investigaciones Científicas y Técnicas (CONICET), Rosario, Argentina, ² Facultad de Ciencias Bioquímicas y Farmacéuticas, Universidad Nacional de Rosario (UNR), Rosario, Argentina, ³ Laboratório de Ultraestrutura Celular Hertha Meyer, Instituto de Biofísica Carlos Chagas Filho, Universidade Federal do Rio de Janeiro, Rio de Janeiro, Brazil, ⁴ Instituto Nacional de Ciência e Tecnologia em Biologia Estrutural e Bioimagens, Rio de Janeiro, Brazil, ⁵ Facultad de Ciencias Médicas, Universidad Nacional de Rosario (UNR), Rosario, Argentina

Trypanosomatids have a cytoskeleton arrangement that is simpler than what is found in most eukaryotic cells. However, it is precisely organized and constituted by stable microtubules. Such microtubules compose the mitotic spindle during mitosis, the basal body, the flagellar axoneme and the subpellicular microtubules, which are connected to each other and also to the plasma membrane forming a helical arrangement along the central axis of the parasite cell body. Subpellicular, mitotic and axonemal microtubules are extensively acetylated in *Trypanosoma cruzi*. Acetylation on lysine (K) 40 of α -tubulin is conserved from lower eukaryotes to mammals and is associated with microtubule stability. It is also known that K40 acetylation occurs significantly on flagella, centrioles, cilia, basal body and the mitotic spindle in eukaryotes. Several tubulin posttranslational modifications, including acetylation of K40, have been cataloged in trypanosomatids, but the functional importance of these modifications for microtubule dynamics and parasite biology remains largely undefined. The primary tubulin acetyltransferase was recently identified in several eukaryotes as Mec-17/ATAT, a Gcn5-related N-acetyltransferase. Here, we report that *T. cruzi* ATAT acetylates α -tubulin *in vivo* and is capable of auto-acetylation. TcATAT is located in the cytoskeleton and flagella of epimastigotes and colocalizes with acetylated α -tubulin in these structures. We have expressed TcATAT with an HA tag using the inducible vector pTcINDEX-GW in *T. cruzi*. Over-expression of TcATAT causes increased levels of the alpha tubulin acetylated species, induces morphological and ultrastructural defects, especially in the mitochondrion, and causes a halt in the cell cycle progression of epimastigotes, which is related to an impairment of the kinetoplast division. Finally, as a result of TcATAT over-expression we observed that

parasites became more resistant to microtubule depolymerizing drugs. These results support the idea that α -tubulin acetylation levels are finely regulated for the normal progression of *T. cruzi* cell cycle.

Keywords: tubulin (Microtubules), cytoskeleton, flagella, acetylation, cell division

INTRODUCTION

Trypanosoma cruzi, the etiological agent of Chagas disease or American trypanosomiasis, is a kinetoplastid parasite with a complex life cycle that alternates between a mammalian host and an insect host (Triatominae family), which is the biological vector of this disease. The World Health Organization classifies Chagas disease as one of the 13 most neglected tropical diseases, constituting a very important social and economic problem in Latin America (WHO, 2012; <http://who.int>).

Trypanosomatids have a cytoskeleton arrangement that is simpler than what is found in most eukaryotic cells. However, it is precisely organized and constituted by stable microtubules (MT). Such MTs are present in the mitotic spindle during mitosis, the basal body, the flagellar axoneme and the subpellicular MTs, which are connected to each other and also to the plasma membrane, thus forming a helical arrangement along the central axis of the parasite cell body (Vidal et al., 2017). MTs provide the basis for cytoskeletal architecture and are formed by α/β -tubulin heterodimers, comprising 13 typical protofilaments connected to each other forming helical tubes. These structures are regulated by interacting with a variety of MT-associated proteins (MAPs), also by variable rates of expression of α - and β -tubulin genes and by a plethora of post-translational modifications (PTMs) (Gadadhar et al., 2017). Several conserved lysines in α - and β -tubulin are acetylated in eukaryotes, and acetylation of the α -tubulin luminal residue lysine 40 (K40) has been the most characterized since its discovery over thirty years ago (L'Hernault and Rosenbaum, 1985; Al-Bassam and Corbett, 2012; Kull and Sloboda, 2014; Eshun-Wilson et al., 2019). Acetylation of α -tubulin on K40 was associated with the stability of microtubules and described as a marker of microtubules resistance to depolymerizing drugs study (L'Hernault and Rosenbaum, 1985; Piperno et al., 1987). In most eukaryotic cells acetylated α -tubulin is a minor isoform, observed in primary cilia, flagella, centrioles and neuronal axons (Piperno et al., 1987; Hubbert et al., 2002; Kalebic et al., 2012; Nakakura et al., 2015). In contrast, trypanosomatids have a significantly high proportion of acetylated α -tubulin, concentrated in the subpellicular, mitotic and axonemal MTs (Sasse and Gull, 1988; Souto-Padron et al., 1993), which makes these organisms attractive models to study the function of α -tubulin K40 acetylation.

Although acetylation typically correlates with stable and long-lived microtubules in cells, acetylation itself does not confer stability, but may rather make microtubules more resilient to mechanical forces (Howes et al., 2013; Szyk et al., 2014; Coombes et al., 2016; Portran et al., 2017). Yet despite years of study, the effects of acetylation on MTs and MT function in cells are still

debated. The primary α -tubulin acetyltransferase was recently identified in several eukaryotes as MEC-17/ATAT, a Gcn5-related N-acetyltransferase containing a catalytic domain that is conserved from protists to mammalian species that use activated acetyl coenzyme A as a common acetyl donor and have diverse substrate specificities (Dyda et al., 2000). MEC-17/ATAT directly promotes α -tubulin acetylation *in vitro* and it is the major α -tubulin acetyltransferase *in vivo* (Akella et al., 2010; Shida et al., 2010). MEC-17 is required for touch sensation in *Caenorhabditis elegans*, normal embryonic development in zebrafish, and the rapid assembly of primary cilia in RPE-hTERT (Human Epithelial cells immortalized with hTERT) cells (Akella et al., 2010; Shida et al., 2010; Li et al., 2012). Also, acetylation does not seem to be only a passive mark on microtubules, as its loss disrupts microtubule structural integrity in touch receptor neurons, leading to axonal morphology defects (Cueva et al., 2012). Loss of ATAT also causes brain abnormalities in mice (Kim et al., 2013). ATAT was characterized in the apicomplexan parasite *Toxoplasma gondii* where it was shown that K40 acetylation stabilizes tachyzoite MTs and is required for daughter cell formation and karyokinesis. *TgATAT* is expressed in a cell cycle-regulated manner and genetic disruption ablates K40 acetylation, thus inducing replication defects, since parasites appear to initiate mitosis but exhibit an incomplete or improper nuclear division (Varberg et al., 2015).

Several tubulin PTMs, including acetylation of K40, have been cataloged in trypanosomatids (Rosenzweig et al., 2008; Nett et al., 2009; Tsigankov et al., 2013; Moretti et al., 2018), but the functional importance of these modifications for MT dynamics and parasite biology remains largely undefined. In this work we have studied the effect of α -tubulin hyperacetylation on *T. cruzi* cell cycle by over-expressing its α -tubulin acetyltransferase (*TcATAT*) using the tetracycline-inducible vector pTcINDEX-GW (Alonso et al., 2014a). This system allowed us to control the amount of *TcATAT*, and hence the amount of acetylated α -tubulin in epimastigotes. Over-expressing parasites showed an increase of acetylated α -tubulin as expected that was associated to growth defects related to a cell cycle arrest and impairment of kinetoplast division. *TcATAT* is located in the cytoskeleton and flagella of *T. cruzi* and colocalizes with acetylated α -tubulin. Over-expression also induced morphological alterations that are related to cell division impairment, and ultrastructural changes, especially in the mitochondrial branches and in kDNA topology. These evidence supports the idea that α -tubulin acetylation is tightly regulated in *T. cruzi* and indicates that although the cytoskeleton arrangement is considered stable in trypanosomatids, a dynamic instability of microtubules is required for replication and cell cycle progression.

MATERIALS AND METHODS

Molecular Cloning of *Tc*ATAT-HA

*Tc*ATAT gene from *T. cruzi* Dm28c strain were amplified using the following oligonucleotides, TATFw : AAGGATTCATGTA TCCGATGATGTCCCGATTATGCTAGTTCACATCG CAA and TATRv : AACTCGAGTGTCTGGAGTACCACT, adding and HA-tag in the N-terminus (in bold). DNA purified from *T. cruzi* Dm28c epimastigotes was used as template. The PCR products obtained with a proofreading DNA polymerase were inserted into pCR2.1-TOPO vector (Invitrogen) and sequenced. *Tc*ATAT-HA coding regions was then inserted into a pENTR3C vector (Gateway system, Invitrogen) using the *Bam*HI/*Xho*I restriction sites included in the oligonucleotides (underlined) and then transferred to pDEST17 (Gateway system, Invitrogen) and p*Tc*INDEX-GW vectors by recombination using LR clonase II enzyme mix (Invitrogen). The pDEST17 constructs were transformed into *Escherichia coli* BL21 pLysS and recombinant proteins, fused to a six histidine-tag, were obtained by expression-induction with 0.5 mM IPTG for 3 h at 30°C. The proteins were purified by affinity chromatography using a Ni-NTA agarose resin (Qiagen) following the manufacturer's instructions. The purity of the purified recombinant protein was assessed by SDS-PAGE and Coomassie staining (**Supplementary Figure 1A**). Before using this protein for antibody generation in rabbits (*Polyclonal Antibodies*), the band corresponding to ATAT-6xhis were electroeluted.

Trypanosoma cruzi Culture and Transfection

T. cruzi Dm28c epimastigotes were cultured at 28°C in LIT medium (5 g/L liver infusion, 5 g/L bacto-tryptose, 68 mM NaCl, 5.3 mM KCl, 22 mM Na₂HPO₄, 0.2% (w/v) glucose and 0.002% (w/v) hemin) supplemented with 10% (v/v) heat-inactivated, UV-irradiated Fetal Calf Serum (FCS) (Internegocios S.A, Argentina). Viability was determined by counting live cells with a haematocytometer using Erythrosin B staining (Campos et al., 2011; Kim et al., 2016). For half media inhibitory concentration (IC₅₀) calculations parasites were treated with Oryzalin (0–300 μM) for 72 h. and the number of parasites was plotted against the log[Oryzalin]. The plot was fitted with the non-parametric regression log(inhibitor) vs. response -Variable slope (four parameters) in GraphPad Prism version 8.0.

Epimastigotes' motility was examined using the computer-assisted semen analysis (CASA) system (Microptic, SCA evolution). Parameters used were as follows: 30 frames acquired, frame rate of 60 Hz, and cell size of 10–100 μm². At least 30 microscopy fields corresponding to a minimum of 300 epimastigotes were analyzed in each experiment.

Epimastigotes from *T. cruzi* Dm28c were transfected with the pLEW13 plasmid to generate parasites expressing T7 RNA polymerase and the tetracycline repressor using a nucleofection method. Briefly, epimastigotes were cultured in LIT medium at 28°C to a final concentration of 4x10⁷ parasites per transfection. Then, parasites were harvested by centrifugation at 1500 g for 10 min at room temperature, washed once with phosphate buffered saline (PBS) and resuspended in 0.4 ml BSF transfection buffer (5 mM KCl, 0.15 mM CaCl₂, 90 mM

Na₂HPO₄, 50 mM HEPES pH 7.3). Nucleofection (Nucleofector 2B, Lonza) was performed in a 0.2 cm gap cuvette (Bio-Rad) with ~20 μg of plasmid DNA added to a final volume of 400 μl. The parasite-DNA mixture was kept on ice for 20 min prior to nucleofection with program X-014. After nucleofection, cells were transferred into 3 ml of LIT medium containing 20% FCS, maintained at room temperature for 15 min and then incubated at 28°C. Geneticin (G418; Life Technologies) was added at a concentration of 200 μg/ml, and parasites were incubated at 28°C. After selection, pLEW13 transfected epimastigotes were maintained in the presence of 100 μg/ml of G418 (Sigma Aldrich). This parental cell line was then nucleofected with p*Tc*INDEX-GW *Tc*ATAT-HA construct following a similar protocol and transgenic parasites were obtained after 4 weeks of selection with 100 μg/ml G418 and 200 μg/ml Hygromycin B (Sigma Aldrich).

Polyclonal Antibodies

All experiments were approved by the Institutional Animal Care and Use Committee of the School of Biochemical and Pharmaceutical Sciences, National University of Rosario (Argentina) (File 6060/227) and conducted according to specifications of the US National Institutes of Health guidelines for the care and use of laboratory animals. Rabbits were only used for the production of antiserum. A rabbit was immunized two times with recombinant ATAT-HA protein purified from *E. coli* and an equal volume of Freund's adjuvant. The animal was bled two weeks after the final injection.

Protein Extracts

Exponentially growing epimastigotes were washed twice with cold PBS, and the pellets were resuspended in lysis buffer (20 mM HEPES, 8 M Urea) and incubated for 30 min at room temperature with gentle agitation. Insoluble debris was eliminated by centrifugation. The same procedure was applied to amastigote and trypomastigote cellular pellets. *T. cruzi* cytoskeleton-enriched extracts were prepared as previously described (Alonso et al., 2014b).

Western Blot

Protein extracts were fractioned in SDS-PAGE and transferred to a nitrocellulose membrane. Transferred proteins were visualized with Ponceau S staining. Membranes were treated with 10% non-fat milk in PBS for 2 h and then incubated with specific antibodies diluted in 0.5% Tween 20 in PBS (PBS-T) for 3 h. Primary antibodies used were: rat monoclonal anti-HA 1:2000 (ROCHE), affinity-purified rabbit polyclonal anti-*Tc*ATAT 1:200, mouse monoclonal anti-trypanosome α-tubulin clone TAT-1 1:1000 (a gift from K. Gull, University of Oxford, UK), rabbit polyclonal anti-Acetyl-lysine 1:1000 (Millipore), mouse monoclonal anti-acetylated α-tubulin clone 6-11B-1 1:2000 (Sigma Aldrich). Bound antibodies were detected using peroxidase-labeled anti-rabbit IgG (GE Healthcare), anti-mouse IgG (GE Healthcare) or anti-rat IgG (Thermo Scientific) and developed using ECL Plus kit (GE Healthcare) according to manufacturer's protocols. Immunoreactive bands were visualized and photographed in the Amersham Imager 600

(GE Healthcare). Images were processed and bands were quantified with ImageJ (Schindelin et al., 2012).

Preparation of Cytoskeletal and Flagellar Complexes

The isolated cytoskeletons and flagellar complexes were obtained as previously described (Alonso et al., 2016) and followed by the immunofluorescence protocol as described below.

Immunofluorescence

Trypomastigotes and exponentially growing epimastigotes were centrifuged, washed twice in PBS, settled on polylysine-coated (Sigma Aldrich) coverslips and fixed with 4% para-formaldehyde in PBS at room temperature for 20 min. For the mitochondrial staining, epimastigotes were resuspended in PBS and incubated with 1 μ M MitoTracker Orange CMTMRos (Invitrogen) for 30 min at 28°C, washed twice in PBS and fixed with 4% para-formaldehyde. Fixed parasites were washed with PBS and permeabilized with 0.1% Triton X-100 in PBS for 10 min. After washing with PBS, parasites were incubated with the appropriate primary antibody diluted in 5% BSA in PBS for 2 h at room temperature. Primary antibodies used were: rat monoclonal anti-HA 1:200 (ROCHE), affinity-purified rabbit polyclonal anti-*Tc*ATAT 1:20, mouse monoclonal anti-acetylated α -tubulin clone 6-11B-1 1:100 (Sigma Aldrich) and mouse polyclonal anti-PAR2 1:100 (*T. cruzi* paraflagellar rod 2 protein) (Saborio et al., 1989). In colocalization experiments both antibodies were incubated together. Non-bound antibodies were washed with 0.01% Tween 20 in PBS and then the slides were incubated with fluorescent-conjugated anti-mouse Alexa-555 (Invitrogen) or anti-rat (FITC, Invitrogen) and anti-rabbit (FITC, Jackson Immuno Research) IgG antibodies and 2 μ g/ml of DAPI for 1 h. The slides were washed with 0.01% Tween 20 in PBS and finally mounted with VectaShield (Vector Laboratories). Images were acquired with a confocal Zeiss LSM880 and Nikon Eclipse Ni-U epifluorescence microscope. ImageJ software were used to process all images.

Ultrastructural Analysis

Scanning Electron Microscopy (SEM)

Cells were fixed in 2.5% glutaraldehyde diluted in 0.1 M cacodylate buffer (pH 7.2) for 1 h, following washes in the same buffer and then adhered to poly-L-lysine-coated microscope coverslips. After fixation, parasites were post-fixed with 1% osmium tetroxide diluted in cacodylate buffer for 1 h, dehydrated in ethanol (50%, 70%, 90%, and two exchanges of 100%, 10 min in each step), critical point dried in CO₂ by using a Leica EM CPD030 equipment (Leica, Wetzlar, Germany) and ion sputtered in a Balzers FL9496 unit (Postfach 1000 FL-9496 Balzers Liechtenstein). Samples were observed under an EVO 40 VP SEM (Zeiss, Germany).

Transmission Electron Microscopy (TEM)

Conventional technique: Cells were fixed as described for Scanning electron microscopy. Then, samples were post-fixed in 1% osmium tetroxide and 0.8% potassium ferricyanide, diluted in the same buffer, for 1 h. After this, parasites were

washed in cacodylate buffer, dehydrated in a graded series of acetone (50%, 70%, 90%, and two exchanges of 100%, 10 min in each step) and embedded in Polybed resin (Epon) (Electron Microscopy Sciences, Hatfield, PA, USA). Ultra-thin sections were stained with uranyl acetate for 40 min and then with lead citrate for 5 min. Samples were observed under a Jeol 1200 EX TEM operating at 80 kV (Jeol, Japan).

Ultrastructural Cytochemistry – EDTA technique (Bernhard, 1969): Parasites were fixed in glutaraldehyde and then dehydrated in ethanol, as described for Scanning electron microscopy. After this, samples were embedded in Polybed resin (Epon) (Electron Microscopy Sciences, Hatfield, PA, USA). Ultrathin sections were stained in the following sequence: 5% uranyl acetate for 5 min, 0.2 M EDTA, pH 7.0, for 45 min and lead citrate for 1 min. This regressive stain removes the uranyl acetate bound to deoxyribonucleoproteins but not from ribonucleoproteins. After this procedure, areas containing DNA appear bleached after EDTA treatment, whereas those containing RNA remain stained. Thus, this technique has been applied to reveal nuclear domains containing ribosomes (Cavalcanti et al., 2008).

Cell Cycle Analysis

Synchronization of epimastigotes in G1 of the cell cycle was achieved using hydroxyurea (HU) (Fassolari and Alonso, 2019). Cells in exponential growth phase were arrested by incubation with 20 mM of HU for 24 h and then released by washing twice with PBS and suspending the cells in culture medium. Cells continued to be cultured for 24 h and samples were taken at the indicated time points. Cell cycle progression of parasites and the analysis by flow cytometry was carried out as previously described (Tavernelli et al., 2019). Briefly, at each time point one million cells were fixed with cold 70% ethanol and then washed with PBS and stained with 20 μ g/ml Propidium Iodide (PI) in buffer K (0.1% sodium citrate, 0.02 mg/ml RNase A (Sigma), and 0.3% NP-40). Ten thousand events per sample were acquired using BD Cell Sorter BD FACSaria II. Results were analyzed with FlowJo software. Cell number was plotted, and the presented data is a mean \pm S.D. of three independent cell cultures. Plots represent one of three independent experiments performed.

ATAT-HA Purification from *T. cruzi* Epimastigotes

A culture of 50 ml of *T. cruzi* Dm28c p*Tc*INDEX-GW-ATAT-HA induced with 0.5 μ g/mL tetracycline for 24 h was collected and resuspended in 500 μ l lysis buffer MME (Mops pH 6.9 10 mM, EGTA-EDTA 1 mM, MgSO₄ 1 mM) supplemented with NaCl 1M, Triton X-100 0.2% and protease inhibitor cocktail (GE). Cells were incubated with agitation at 4°C for 30 min and then ruptured by sonication and centrifuged for 20 min. at 16,000 g. The supernatant was loaded to an anti-HA agarose column (Roche) following the manufacturers' instructions. The flowthrough was collected, and the column was washed with 1 volume of PBS 0.5% Tween-20. Bound protein were eluted four times with 250 μ l of HA peptide (Sigma-Aldrich) (0,1 mg/ml). The purity of the purified recombinant protein was assessed by SDS-PAGE and Coomassie staining (**Supplementary Figure 1B**).

Autoacetylation Assay

0.5 μg of ATAT-HA purified from *T. cruzi* epimastigotes were incubated in the absence or presence of 0.5 mM Acetyl CoA (Sigma) for 1.5 h at 37°C in acetylation buffer (50mM Tris-HCl, pH 8.0; 10% glycerol; 1mM MgCl_2 ; 1mM DTT; 1mM PMSF; 20 mM sodium butyrate). The samples were resolved on SDS-PAGE gels, transferred to nitrocellulose membranes (GE Healthcare) and subjected to Western blot analysis as described above.

RESULTS

An ATAT Homolog Is Expressed in All *T. cruzi* Life Cycle Stages

A bioinformatic survey of the *T. cruzi* genome in TriTrypDB (<https://tritrypdb.org/>) revealed a single gene containing a MEC-17 domain belonging to the Gcn5-related superfamily (PF05301), described in this database as a putative alpha-tubulin N-acetyltransferase. In the genome of the Dm28c strain the predicted protein sequence is 330 amino-acids long with the acetyltransferase domain in its N-terminal portion (C4B63_12g332), from now on we will name it *TcATAT* (Figure 1). When we looked for homologs in other trypanosomatids, we found that in *T. brucei* (Tb927.3.1400) the putative alpha-tubulin N-acetyltransferase contains 55% of identical residues compared to *T. cruzi* and that this homology is widespread along the sequence. In the case of *Leishmania major* (LmjF.25.1150) the identity is restricted to the acetyltransferase domain (50% identical residues) (Supplementary Figure 2A). When we aligned the acetyltransferase domains of ATAT homologs from several representative species with Clustal Omega, we observed that the acetyltransferase domain is highly conserved, including the key residues critical for the enzymatic activity (asterisks in Figure 1B), while both N-terminal and C-terminal portions of the different homologs are highly dissimilar and even have different lengths (Figure 1A). For example, the *Toxoplasma gondii* ATAT is considerably larger than all previously characterized ATAT/MEC-17 proteins (Varberg et al., 2015).

RNAseq experiments showed that *TcATAT* transcripts are more abundant in trypomastigote stage compared to epimastigote stage (Smircich et al., 2015) and that they peak in late amastigote and trypomastigote stages (Li et al., 2016). To assess the expression pattern of *TcATAT* in all the three stages of *T. cruzi* life cycle we obtained polyclonal antibodies from rabbit against the recombinant protein that were purified and used in Western blot and immunofluorescence assays in epimastigotes, amastigotes and trypomastigotes. We observed that *TcATAT* is expressed in all life cycle stages, located in the whole cell body of *T. cruzi* and apparently excluded from the nuclei (Figure 1C). Some discrete spots throughout the cytoplasm in epimastigotes and amastigotes were also observed (Figure 1C, white arrowheads). As expected, we detected *TcATAT* by Western blot in whole extracts of epimastigotes, trypomastigotes and amastigotes, with a higher expression in the last stage (Figure 1D).

TcATAT-HA Has Acetyltransferase Activity and Acetylates α -Tubulin in the Cytoskeleton and Flagellum of Epimastigotes

To determine the impact of *TcATAT* on α -tubulin acetylation we obtained *T. cruzi* epimastigotes stably transfected with the p*TcINDEX*-GW vector (Alonso et al., 2014a) bearing the ATAT coding sequence with a hemagglutinin tag on its N-terminus (HA). This plasmid allowed us to induce the expression of the transgene with tetracycline (Taylor and Kelly, 2006). We corroborated the over-expression of *TcATAT*-HA in epimastigotes by immunofluorescence and Western blot assays with anti-HA antibodies 24 h post-induction (p.i.) (Figures 2A, B), and we did not detect tagged protein without tetracycline induction (Figure 2B and Supplementary Figure 3). At this time, an evident morphological defect was detected in the induced parasites (Figure 2A, arrowhead) and a round refringent structure was observed in a proportion of the over-expressing epimastigotes.

Then, we quantified the amount of acetylated α -tubulin at different induction times by densitometry (Figure 2C) in the over-expressing epimastigotes. The amount of acetylated α -tubulin increased with *TcATAT*-HA induction time being almost 10 times higher at 24 h.p.i. compared to the uninduced control. ATAT shows autoacetylation activity in other organisms (Kalebic et al., 2012; Zhou et al., 2018) and *TcATAT* was predicted to be acetylated on K263 with the PAIL server (Deng et al., 2016). To study if this *TcATAT* undergoes autoacetylation we performed an autoacetylation assay using purified *TcATAT*-HA from epimastigotes incubated in the absence or presence of Acetyl-CoA. We detected acetylated *TcATAT* only in the presence of Acetyl-CoA confirming that *TcATAT* has a fully functional domain with acetyltransferase activity (Figure 2D).

We also tested whether ATAT-HA overexpressing epimastigotes were more resistant to the microtubule-disrupting drug Oryzalin to correlate alpha tubulin acetylation with stability. Oryzalin effect on *T. cruzi* has not been reported yet, but we found in the literature that a similar dinitroaniline, Trifuralin, had an IC_{50} between 70 and 160 μM depending on the strain used (Traub-Cseko et al., 2002). To begin with, we determined Oryzalin IC_{50} in Dm28c epimastigotes (250.5 μM) and found that it was higher than what was reported for Trifuralin (Supplementary Figure 4A). Epimastigotes treated with Oryzalin show a dose-dependent loss of normal morphology: at higher concentrations epimastigotes adopt a rounded shape with a shorter flagellum, perhaps due to alterations in the polymerization of axonemal microtubules (Supplementary Figure S4B). In presence of 200 μM Oryzalin, Dm28c p*TcINDEX*-GW ATAT-HA epimastigotes induced with tetracycline grew better than uninduced parasites (without tetracycline: 67% growth and with tetracycline: 85% (***) growth), as expected for an increased amount of acetylated α -tubulin.

To better characterize the localization of *TcATAT*, we isolated subpellicular microtubules and flagellar complexes from transfected epimastigotes and analyzed the presence of

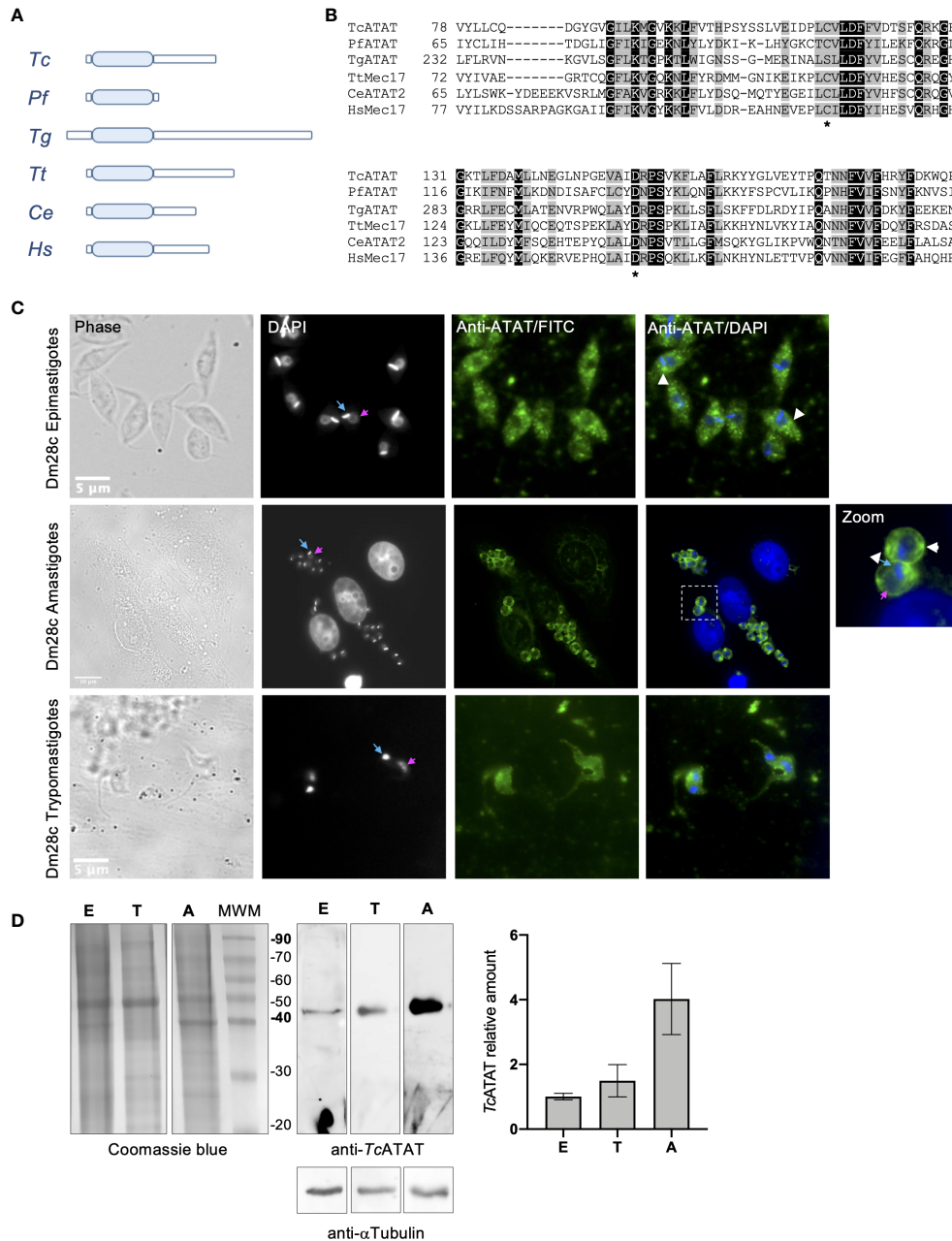


FIGURE 1 | The GCN5 acetyltransferase domain is conserved in *T. cruzi*. **(A)** Schematic representation of ATAT/Mec17 from different organisms (in order: *T. cruzi*, *Plasmodium falciparum*, *Toxoplasma gondii*, *Tetrahymena thermophila*, *Caenorhabditis elegans*, *Homo sapiens*). The acetyltransferase domain is represented as light blue rectangles. **(B)** Multiple sequence alignment of the acetyltransferase domain using T-coffee and colored with Boxshade. Two conserved residues important for catalysis in *HsATAT* are marked with asterisks. Accession number for the sequences used: *Tc*, TCDM_08085; *Pf*, PF3D7_0924900; *Tg*, TGME49_31600; *Tt*, TTHERM_00355780; *Ce*, CELE_W06B11.1; *Hs*, XP_005249477.1. *TcATAT* is expressed in all life cycle stages of *T. cruzi*. **(C)** Immunolocalization of *TcATAT* in Dm28c epimastigotes, amastigotes and trypomastigotes using rabbit polyclonal anti-*TcATAT* antibodies. Bar: 10 μ m. DAPI was used as nucleus and kinetoplast marker. The light blue arrow indicates the kinetoplast and the pink arrow indicates the nucleus. **(D)** Total extracts of Dm28c epimastigotes (E), trypomastigotes (T) and amastigotes (A) were separated by SDS/PAGE and stained with Coomassie Blue (left panel), followed by Western blot analysis using rabbit monoclonal anti-*TcATAT* antibodies and mouse monoclonal anti- α -tubulin (anti- α Tubulin) (right panel). Bands were quantified by densitometry using α -tubulin signal to normalize the amount of *TcATAT* and plotted. The amount of *TcATAT* in was normalized using the amount in epimastigotes as 1.

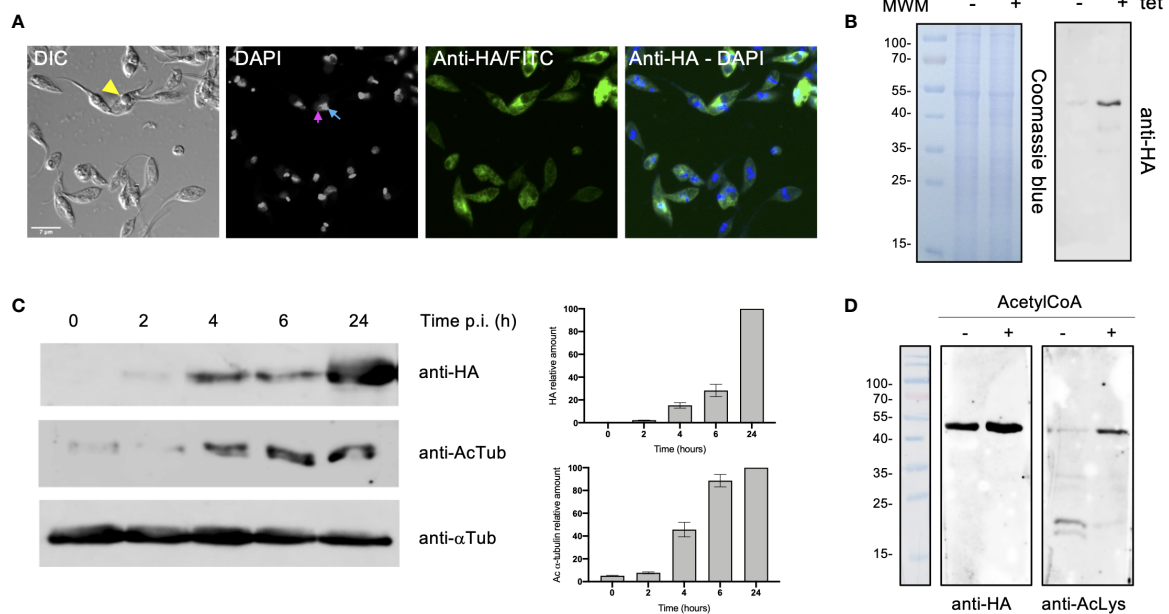


FIGURE 2 | Over-expression of ATAT-HA in epimastigotes increases α -tubulin acetylation. **(A)** Immunolocalization of ATAT-HA with rat monoclonal anti-HA antibodies in Dm28c p7cINDEX-GW ATAT-HA epimastigotes induced with 0.5 μ g/ml tetracycline for 24 h. Bar: 5 μ m. DAPI was used as nucleus and kinetoplast marker. The light blue arrow indicates the kinetoplast and the pink arrow indicates the nucleus. **(B)** Total extracts of p7cINDEX-GW ATAT-HA epimastigotes in the absence (-) or presence (+) of 0.5 μ g/ml tetracycline for 24 h were separated by SDS/PAGE and stained with Coomassie Blue (left panel), followed by Western blot analysis using rat monoclonal anti-HA antibodies (right panel). **(C)** Western blot of total extracts of p7cINDEX-GW ATAT-HA epimastigotes with 0.5 μ g/ml tetracycline a different time points post-induction using rat monoclonal anti-HA, mouse monoclonal anti-acetylated α -tubulin (anti-AcTub), rabbit monoclonal anti-*Tc*ATAT antibodies and mouse monoclonal anti- α -tubulin (anti- α Tub). Bands were quantified by densitometry using α -tubulin signal to normalize the amount of ATAT-HA and acetylated α -tubulin (right panel). Plots represent one of three independent experiments performed. **(D)** ATAT-HA autoacetylation assay. ATAT-HA was purified from *T. cruzi* epimastigotes and incubated in the absence (-) and presence (+) of AcetylCoA and then separated by SDS/PAGE followed by Western blot analysis with rat monoclonal anti-HA antibodies and rabbit monoclonal anti-Acetylated Lysine (anti-AcLys).

*Tc*ATAT-HA in these structures. As observed in **Figure 3A**, ATAT-HA colocalizes with acetylated α -tubulin in the subpellicular microtubules and the flagellar axoneme. The round structures observed by light microscopy remains insoluble after treatment with detergent and NaCl and is labeled with the anti-HA/FITC antibody (**Supplementary Figure S5A**). In intact epimastigotes fixed with paraformaldehyde confocal microscopy *Tc*ATAT-HA labeling was more intense at the surroundings of these round structures (**Figure 2A**). We performed a Z-stack confocal imaging and 3D reconstruction (**Supplementary movie V1**) and observed that *Tc*ATAT-HA formed a ball-like structure near the nucleus and the kinetoplast.

Immunolocalization of acetylated α -tubulin was more intense at the cell periphery in non-induced cells, however in over-expressed parasites labeling became spread all over the cytoplasm (**Supplementary Figure S5B**). As a control we verified that *Tc*ATAT-HA did not co-localize with the paraflagellar rod that runs parallel to the axoneme (**Supplementary Figure S5C**). Also, we obtained protein extracts enriched in cytoskeletal and flagellar proteins and observed by Western blot that both the endogenous ATAT and the over-expressed version are only

present in the fraction that corresponds to insoluble cytoskeletal and flagellar proteins (P, in **Figure 3B**), confirming that it is tightly associated to these structures.

The refringent button-like structure observed in the over-expressing parasites was quantified and it was present in approximately 20% of the epimastigotes 48 h.p.i. We also determined that this structure grew with induction time and was usually observed near the nucleus and the kinetoplast (**Figure 4A**). Transmission Electron Microscopy (TEM) analyses revealed that this round structure is electrondense, not delimited by membrane, and sometimes is seen in continuity with the endoplasmic reticulum, resembling an inclusion body (**Figures 4B a-d**). These results correlate with the accumulation of *Tc*ATAT-HA observed in association to the isolated cytoskeleton where the structure is seen connected to the flagellum (**Figure 3A**). Considering that overexpressing cells can produce large amounts of ribosomes, the EDTA technique, which stains areas rich in ribonucleoproteins, was used to verify the nature of this structures. Results showed ribosome subunits in the heterochromatin region, as well as in the granular region of the nucleolus, whereas the inclusion body-like structure lacks ribosomes and present a distinct electron density in relation to such regions (**Figure 4B e**).

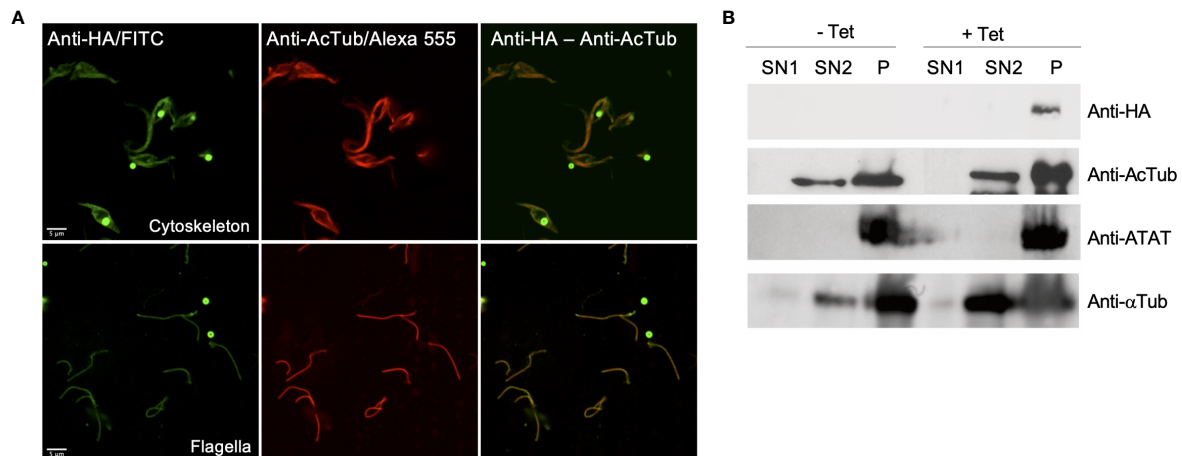


FIGURE 3 | ATAT-HA colocalizes with acetylated α -tubulin in the cytoskeleton and flagella of epimastigotes. **(A)** Immunolocalization of ATAT-HA with rat monoclonal anti-HA antibodies and mouse monoclonal anti-acetylated α -tubulin (anti-AcTub) in isolated cytoskeletons and flagella of Dm28c pTcINDEX-GW ATAT-HA epimastigotes induced with 0.5 μ g/ml tetracycline for 24 h. **(B)** Extracts enriched in cytoskeletal and flagellar proteins were analyzed by Western blot with rat monoclonal anti-HA antibodies, rabbit polyclonal anti-*Tc*ATAT antibodies, mouse monoclonal anti-acetylated α -tubulin (anti-AcTub) and anti α -tubulin (anti- α Tub). SN1, soluble protein extracts; SN2, soluble cytoskeletal and flagellar protein extracts; P, insoluble cytoskeletal and flagellar protein extracts.

α -Tubulin Hyperacetylation Causes a Halt in the Cell Cycle Progression of Epimastigotes

We performed growth curves of *Tc*ATAT over-expressing epimastigotes in the absence and presence of tetracycline (Figure 5A). A growth impairment was observed after 48 h.p.i. but no differences in viability (measured with Erythrocin B staining) were observed along the entire growth curve (Supplementary Figure S6A). We have previously ruled out any undesired effect of the tetracycline treatment on epimastigote growth (Ritagliati et al., 2015a). We also quantified epimastigotes' motility using CASA software and observed less motile parasites when epimastigotes were induced for 48 h. (Supplementary Figure S6B). Over-expression was also verified with rabbit polyclonal anti-ATAT antibodies in 24 and 48 h.p.i. cells, when the *Tc*ATAT labeling was particularly strong and excluded from the nucleus and kinetoplast (Figure 5B). After 24 h.p.i. parasites that appear to have two nuclei start to accumulate (Zoom in Figure 5B, yellow arrow heads indicate parasites with an aberrant DNA content). Also, localization of *Tc*ATAT changes with over-expression, the discrete spots observed for the endogenous protein are less evident and labeling seems more intense around the nucleus/kinetoplast area.

The cell cycle progression of *Tc*ATAT overexpressing epimastigotes was analyzed by flow cytometry with Propidium iodide (PI) staining for 24 h.p.i. in synchronized epimastigotes (Figure 6A). As expected, in the absence of tetracycline we observed that the cell cycle progressed normally. At time point 0 the main peak corresponds to the parasites on G1 phase of the cell cycle (~60% of the total) that is, parasites with the DNA content corresponding to one nucleus. A second minor peak

represents the parasites in G2/M phase (~30%), which corresponds to epimastigotes with the double of DNA content, including those on cytokinesis. In the valley between the two peaks are the cells on S phase (~10%). Then, at time point 6 h the count of parasites in S phase starts to increase and at 12 h more than half of the parasites are in G2/M phase. Finally, at 24 h, the parasites return to G1 phase. When tetracycline is added the peak of cells in S phase doubles at 12 h.p.i. Furthermore, G2/M peak increased about 20% at 24 h.p.i., suggesting that the *Tc*ATAT overexpression results in an arrest of cells that are dividing and cells that have duplicated their DNA (Figure 6B). This halt in the cell cycle progression was also observed by Scanning Electron Microscopy (Figure 6C). When parasites are induced with tetracycline for 24 h, ~30% of the cells have two flagella, and it appears that there is an impairment in the cleavage furrow progression and cytokinesis (white arrows, Figures 6C g–i) that correlates with the higher proportion of cells in G2/M phase.

As a control, we quantified the population of epimastigotes with two nuclei and one kinetoplast 24 and 48 h.p.i. in an asynchronous population. The ordered progression of the cell cycle, in which kinetoplast segregation precedes nuclear division, allows the identification of three normal states regarding nuclear/kinetoplast (N/K) content: 1N1K, 1N2K, and 2N2K. Under normal conditions, most epimastigotes in a non-synchronous exponentially growing culture contain one nucleus and one kinetoplast (1N1K, usually ~80–95%), corresponding to parasites in G1 or S phase of the cell cycle. A smaller proportion exhibits two kinetoplasts and one nucleus (1N2K ~5%), these correspond to parasites in G2 phase or the beginning of mitosis. Finally, cells presenting two kinetoplasts and two nuclei (2N2K ~3%) are those that have completed mitosis and

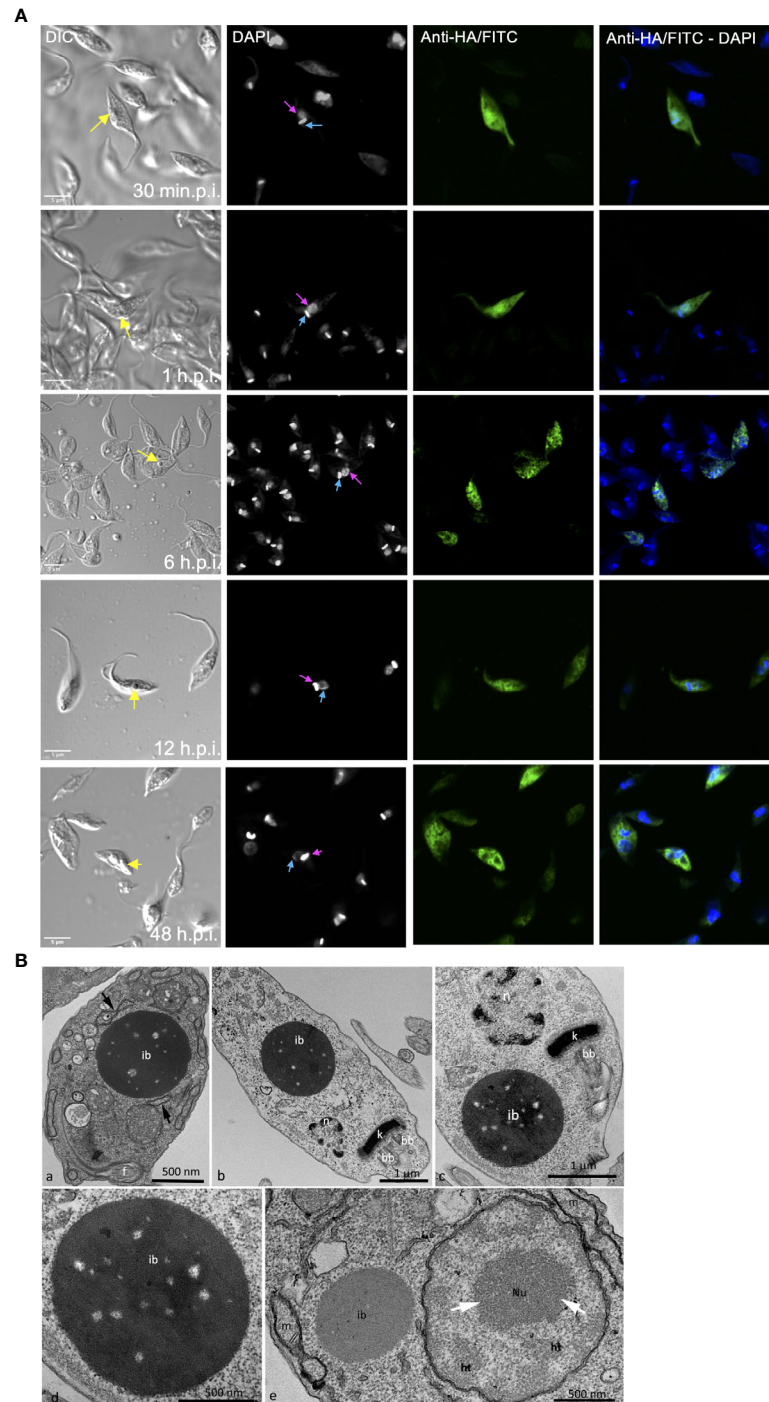


FIGURE 4 | Over-expression of ATAT-HA induced the formation of an inclusion body-like structure. **(A)** Immunolocalization of ATAT-HA with rat monoclonal anti-HA antibodies in Dm28c p7cINDEX-GW ATAT-HA epimastigotes induced with 0.5 mg/ml tetracycline at different time points p.i. The yellow arrow indicates the inclusion body-like structure, the light blue arrow indicates the kinetoplast and the pink arrow indicates the nucleus. DAPI was used as nucleus and kinetoplast marker. Bar: 5 μ m. **(B)** Transmission Electron Microscopy of Dm28c p7cINDEX-GW ATAT-HA epimastigotes induced with 0.5 μ g/ml tetracycline for 48 h. ib, inclusion body-like structure. This structure was seen in close proximity with the endoplasmic reticulum (a, arrows) and was positioned close to the nucleus (n) and the kinetoplast (k) in the posterior part of the cell body (b) or more commonly at the anterior end, close to the kinetoplast and the basal body (c). The inclusion body is not surrounded by a membrane unit (d). bb, basal body; f, flagellum. The EDTA technique revealed ribosome rich regions in the nucleus, as the heterochromatin (ht) and granular domain of the nucleolus (white arrows), whereas the inclusion body-like structure (ib) lacks ribosomes and is less electron-dense in relation to these regions. When comparing the inclusion body-like structure with organelles, as the nucleus (n) and the mitochondrion (m), it is clear that the first one is not surrounded by membrane units (e).

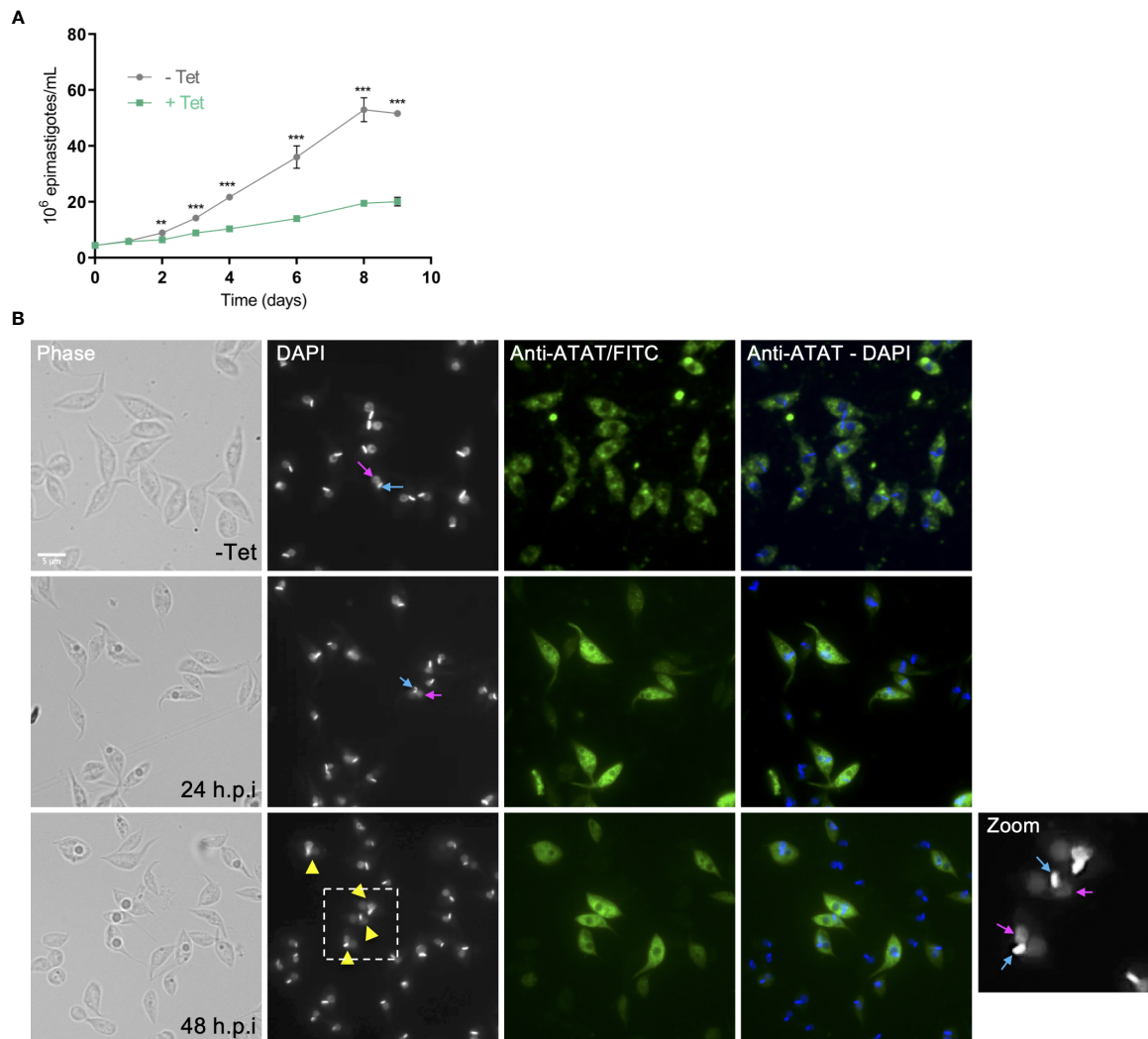


FIGURE 5 | ATAT-HA over-expression negatively impacts on epimastigotes growth. **(A)** Growth curve of Dm28c p7cINDEX-GW ATAT-HA epimastigotes in the absence (grey circles) and presence (green squares) of 0.5 $\mu\text{g/ml}$ tetracycline for 9 days. $**p < 0.005$, $***p < 0.001$ (Student's t-test). The number of epimastigotes per ml was plotted, and the presented data is the mean \pm S.D. of three parallel independent cell cultures. The plot represents one of three experiments performed. **(B)** Immunolocalization of 7cATAT, in Dm28c p7cINDEX-GW ATAT-HA epimastigotes in the absence and presence of 0.5 $\mu\text{g/ml}$ tetracycline for 24 and 48 h. Bar: 5 μm . DAPI was used as nucleus and kinetoplast marker. The light blue arrow indicates the kinetoplast and the pink arrow indicates the nucleus. Yellow arrowheads indicate parasites with an aberrant DNA content.

are undergoing cytokinesis or ready to do so (Elias et al., 2007). Thus, the appearance of cells with abnormal N/K content is indicative of cell cycle impairment. 20% to 30% more parasites with 1K/2N are found in over-expressing conditions than in the uninduced control (Supplementary Figure S8).

Over-Expression of *TcATAT*-HA Alters Acetylated α -Tubulin Distribution and Causes Modifications on Mitochondrion Ultrastructure

Parasites with over-expression of *TcATAT*-HA presented alterations on acetylated α -tubulin distribution observed with

anti-acetylated α -tubulin antibodies. Part of the population accumulates acetylated α -tubulin around the kinetoplast (Figure 7A, yellow arrowheads) and in some parasites it is surrounding the inclusion body-like structure (Figure 7A, white arrowheads).

Trypanosomatids have a single and ramified mitochondrion with the kDNA concentrated in the kinetoplast. The kinetoplast is connected to the basal body that nucleates the flagellum, that are both MT-containing structures. Since the basal body is linked to the kinetoplast by the tripartite attachment complex (TAC) (Kaser et al., 2014), we decided to investigate the mitochondrial morphology and ultrastructure in *TcATAT*-HA over-expressing

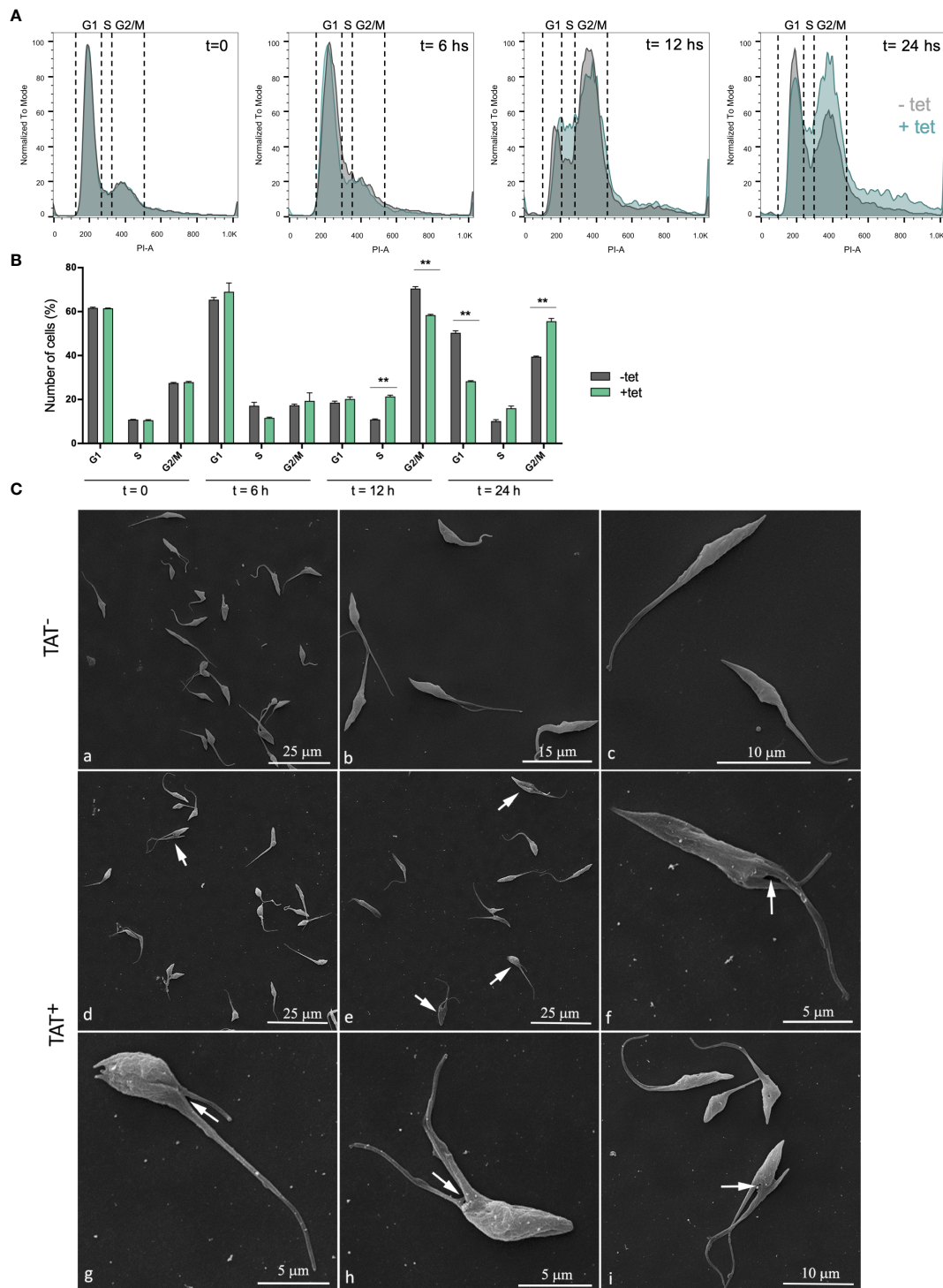


FIGURE 6 | Hyperacetylation alters the cell cycle progression. **(A)** Flow cytometry analysis of synchronized Dm28c p7cINDEX-GW ATAT-HA epimastigotes in the absences (grey) and presence (green) of 0.5 μ g/ml tetracycline at different time points. Histograms are plotted as the normalized number of events vs. propidium iodide absorbance (PI-A). **(B)** Bar graph with the percentages of cells in the different phases of the cell cycle. ** $p < 0.005$ (Student's t test). Cell number was plotted, and the presented data is the mean \pm S.D. of three parallel independent cell cultures. Plots represent one of three experiments performed. **(C)** Images obtained by Scanning Electron Microscopy (SEM) of Dm28c p7cINDEX-GW ATAT-HA. Uninduced epimastigotes (TAT-) (a-c). Parasites induced with 0.5 μ g/ml tetracycline for 24 h (TAT+) (d-i). Induced cells presented a phenotype that indicates cytokinesis arrest (d-e, arrows) and the interruption in the progression of the cleavage furrow (f-i, white arrows).

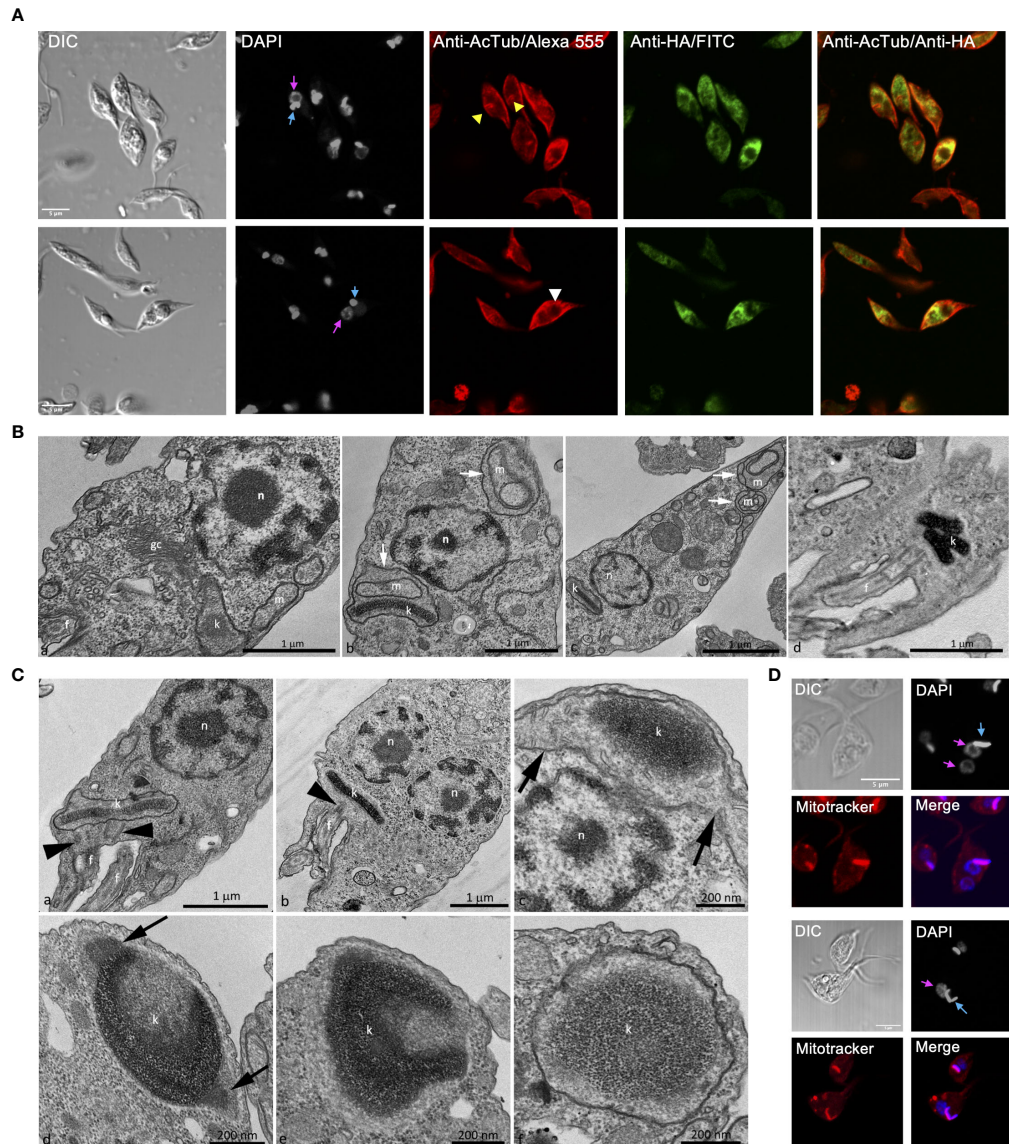


FIGURE 7 | Over-expression *Tc*ATAT-HA causes phenotypic alterations in acetylated α -tubulin distribution and on mitochondrion ultrastructure of epimastigotes. **(A)** Immunolocalization of ATAT-HA with rat monoclonal anti-HA antibodies and mouse monoclonal anti-acetylated α -tubulin (anti-AcTub) of Dm28c p7cINDEX-GW ATAT-HA epimastigotes induced with 0.5 μ g/ml tetracycline for 24 h. Bar = 5 μ m. DAPI was used as nucleus and kinetoplast marker. The light blue arrow indicates the kinetoplast and the pink arrow indicates the nucleus. Yellow arrowheads indicate accumulation of acetylated α -tubulin around the kinetoplast and the white arrowhead indicates accumulation of acetylated α -tubulin around the inclusion body-like structure. **(B)** Transmission Electron Microscopy of Dm28c p7cINDEX-GW ATAT-HA epimastigotes induced with 0.5 μ g/ml tetracycline for 48 h. A general view showing the nucleus, mitochondrial branches, a small portion of the kinetoplast and the Golgi complex that was seen with its typical ultrastructure, without extended cisterns or space alteration between them (a). It was common to observe parasites presenting alterations in the mitochondrial branches and at the kinetoplast region, especially cristae swelling (b and c, white arrows). Parasites presenting a kinetoplast with multiple and electron-dense networks were also observed (d). Cg – Golgi complex; f, flagellum; k, kinetoplast; m, mitochondrial branches; n, nucleus. Bar = 1 μ m. **(C)** Transmission Electron Microscopy of Dm28c p7cINDEX-GW ATAT-HA. In uninduced epimastigotes the replicated kDNA is contained in a kinetoplast associated to two basal bodies (panel a, black arrowheads). Epimastigotes induced with 0.5 μ g/ml tetracycline for 48 h presented atypical characteristics (b–f). In this case, the replicated kDNA is contained in a kinetoplast associated to a single basal body (b, black arrowhead), which results in kinetoplast division impairment in a cell with two nuclei. The kinetoplast region is continuous with mitochondrial branches (panel c, black arrows). The kDNA replication occurs during the S phase when the antipodal sites contain proteins involved in this process (d, black arrows). Since the kDNA replicates, but the kinetoplast does not divide, the network curves and folds over itself, becoming round and presenting an atypical topology. The kinetoplast shape also changes its format from disk to round (d–f). f, flagellum; k, kinetoplast; n, nucleus. Bars = 1 μ m (a and b), 200 nm (c–f). **(D)** Dm28c p7cINDEX-GW ATAT-HA epimastigotes induced with 0.5 μ g/ml tetracycline for 48 h and stained with Mitotracker CMTMRos. DAPI was used as nucleus and kinetoplast marker. The light blue arrow indicates the kinetoplast and the pink arrow indicates the nucleus. The upper panel shows a parasite with a kinetoplast containing a duplicated kDNA and two nuclei, while the lower panel shows a kinetoplast with an arched kDNA that did not suffer scission. Bar = 5 μ m.

cells by TEM and using Mitotracker Orange CMTMRos. In induced epimastigotes, organelles such as the nucleus and the Golgi complex were not affected (**Figure 7B-a**), however cristae swelling was seen in the kinetoplast region and also in the mitochondrial branches (**Figure 7B**, white arrows in b and c). Moreover, sometimes cells presented a kinetoplast containing multiple networks that are very condensed (**Figure 7B**, white arrow in d) indicating kinetoplast division impairment. Images obtained by TEM confirmed this hypothesis since overexpressing parasites presented duplicated kDNA that did not suffer scission and was seen associated to a single basal body (**Figure 7C**, black arrowheads in b), differently to what was observed in the uninduced condition where cells contained two basal bodies (**Figure 7C**, black arrowheads in a). Furthermore, TEM images revealed that when the kDNA duplicated, but the kinetoplast did not divide, the network became curved, folded over itself, thus acquiring a round shape with an atypical condensation. The kinetoplast shape also changed from disk to a round format (**Figures 7C c-f**). Such kDNA alterations were also observed by confocal microscopy in *TcATAT*-HA over-expressing parasites stained with Mitotracker and DAPI. Parasites presented a single kinetoplast with duplicated kDNA and two nuclei (**Figure 7D**, upper panel), as well an arched kDNA (**Figure 7D**, lower panel).

DISCUSSION

In this study, we address the biological relevance of acetylated α -tubulin in the protozoan pathogen *T. cruzi*. More than 30 years ago it was described that acetylated α -tubulin was the major isotype present in *T. brucei* (Schneider et al., 1987; Sasse and Gull, 1988) and *T. cruzi* (Souto-Padron et al., 1993) subpellicular MTs and flagellar axoneme, but the significance of this finding has not been unraveled yet. We have identified and characterized the acetyltransferase responsible for mediating K40 α -tubulin acetylation in *T. cruzi*, *TcATAT*, and shown that its over-expression conduces to a hyperacetylation of α -tubulin that severely affects the normal progression of the cell cycle in epimastigotes. *ATAT*-HA over-expression also confers epimastigotes resistance to Oryzalin, a depolymerizing drug that targets α -tubulin. Dinitroaniline herbicides such as oryzalin, which was shown to depolymerize plant cell microtubules (Morejohn et al., 1987), also disrupt the microtubules of several protozoa including *Tetrahymena* (Stargell et al., 1992) and parasites such as *Leishmania* spp. (Chan et al., 1991), *Entamoeba* spp. (Makioka et al., 2000), *Cryptosporidium parvum* (Armson et al., 2002), *Toxoplasma gondii* (Stokkermans et al., 1996), *Angomonas deanei*, and *Strigomonas culicis* (Catta-Preta et al., 2015). Interestingly, sensitivity of *T. cruzi* to Oryzalin is significantly higher than for other protists where it was studied, what can be explained by the presence of a L at position 267, instead of a V or I found in *Toxoplasma gondii* (Shaw et al., 2000) and *Tetrahymena thermophila* (Dostál and Libusová, 2014), respectively, among other point mutations found in *T. cruzi* α -tubulin.

Acetylated α -tubulin has been associated with stable structures in eukaryotic cells, localizing to primary cilia,

midbodies, centrioles and subsets of cytoplasmic microtubules in 3T3 and HeLa cells (Piperno et al., 1987) and to flagella axonemes, basal bodies and cytoplasmic microtubules radiating from the basal bodies in *Chlamydomonas reinhardtii* (L'Hernault and Rosenbaum, 1985). In *T. brucei* and *T. cruzi* acetylated α -tubulin is distributed widely throughout all microtubular arrays (Sasse and Gull, 1988; Souto-Padron et al., 1993). This post-translational modification appears to occur during or immediately after microtubule polymerization, and the deacetylation process correlates with depolymerization (Sasse and Gull, 1988). The fact that we observed a resistance to an α -tubulin depolymerizing drug when MTs are hyperacetylated suggests that there is a clear link between acetylation and stabilization in *T. cruzi* as reported in other organisms. Subpellicular microtubules that compose the trypanosomatid cytoskeleton are quite stable structures, but our results suggest that a fine regulation in tubulin polymerization/depolymerization is necessary for the correct progression of the cell cycle and protozoan division.

Early electron microscopy revealed distinct subcellular sites from which microtubules appeared to emanate which were named “microtubule-organizing centers” in eukaryotes (MTOCs). Since then, the exact nature of MTOCs has remained unclear. Microtubules have an inherent structural polarity, with a dynamic plus end and a comparatively stable and slow growing minus end. These characteristics of microtubule minus ends can be influenced *in vivo* by an association with a MTOC that can be broadly defined as sites for microtubule nucleation, stabilization, and/or anchoring (Sanchez and Feldman, 2017). Not much is known about MTOCs in trypanosomatids apart from the fact that subpellicular microtubules have uniform spacing over the entire parasite, presenting their minus ends oriented toward the anterior pole of the cell, the region where the single-copy organelles division starts (Wheeler et al., 2019). Trypanosomes have γ -tubulin and γ -tubulin ring complex proteins, but unfortunately their localization or interrogation of function has not led to the definition of the sites of individual microtubule nucleation within the subpellicular array (Zhou and Li, 2015). We observed that *ATAT* is concentrated in discrete spots in epimastigotes and amastigotes, and that it accumulates mainly in the anterior region when over-expressed. These results as well as the fact that α -tubulin acetylation occurs immediately after microtubules polymerization may suggest that *ATAT* stabilizes the microtubules that form the subpellicular corset when they are nucleating in the MTOC.

The *T. cruzi* cell cycle is characterized by a coordinated duplication of nuclear and kinetoplast DNA during the S phase. After kDNA replication, the kinetoplast assumes a more elongated disk shape and segregates at the beginning of the G2 phase. At this point cells present two basal bodies, both linked to the kDNA network (Elias et al., 2007). TEM analyses revealed that many cells showed an elongated kinetoplast, indicating that the kDNA replication occurred, but not the network scission. This is related to hyperacetylation that also caused a marked halt in G2/M phase of the cell cycle as determined by flow cytometry.

A phenotype related to *Tc*ATAT over-expression is the impaired ingression of the cleavage furrow, resulting in a defect in cytokinesis, an observation that can be associated to an increase in the amount of acetylated α -tubulin (or perhaps to a decrease in the amount of non-acetylated α -tubulin available). The blocked cytokinesis resembles the phenotype of *T. brucei* GTPase Arl2 mutants. Arl2 orthologs in mammals are mitochondrial proteins but in *T. brucei* it appears to be a cytoskeletal protein. Knockdown and over-expression of *Tb*Arl2 modulate the levels of acetylated α -tubulin and inhibits cytokinesis and cleavage furrow progression similar to ATAT-HA over-expression (Price et al., 2010). Furthermore, in *T. brucei* cytokinesis proceeds from the anterior end to the posterior end, with the cleavage furrow starting at the distal tip of the new Flagellum Attachment Zone (FAZ) and proceeding along a fold in the cell. The furrow placement relative to the old and new FAZ guarantees correct inheritance of the basal body, kinetoplasts, and flagellar pocket complexes, but the nuclei must be positioned correctly. Finally, the furrow resolves to a single point of connection between the posterior of one daughter cell and the side of the other daughter. This narrow cytoplasmic bridge can persist while the daughter cells restart the cell cycle, although it is normally resolved (Wheeler et al., 2019). In conclusion, furrow ingression must require some rearrangement of the microtubule array. It is quite possible that an increase in α -tubulin acetylation, as a consequence of ATAT-HA over-expression, somehow promotes the stabilization between kDNA and the basal body (which are also composed by MTs) thus impairing MTs rearrangements and cytokinesis. Basal body replication can be impaired in cells over-expressing ATAT-HA, since protozoa containing duplicated kDNA network, a single basal body and only one flagellum were observed. Unfortunately, we still do not know much about the cell cycle checkpoints of *T. cruzi* epimastigotes, what would enable a deeper discussion about the observed phenomenon.

A refringent button-like structure was visible by optic microscopy that started to grow in a time-dependent manner after induction of ATAT-HA over-expression with tetracycline. This round structure contains ATAT-HA, forming an insoluble and tridimensional structure that remains associated with isolated cytoskeletal and flagellar fractions. This atypical structure is electron-dense and is observed by TEM most of the time in the anterior region, close to the nucleus and kinetoplast. It is not delimited by a membrane unit, which suggests that it could be a cumulus of protein, rich in *Tc*ATAT-HA, reminiscent to an inclusion body. Inclusion bodies are aggregates of misfolded protein known to occur in eucaryotic cells, for example during neurodegenerative disorders (Chung et al., 2018). Inclusion bodies are also found in bacteria as particles of aggregated protein (Singh and Panda, 2005). To our knowledge there are no reports of inclusion bodies in trypanosomatids occurring as a consequence of over-expression of exogenous proteins. It is also worth mentioning that we have used this over-expression systems for different proteins and never observed a similar phenotype (Ritagliati et al., 2015a;

Ritagliati et al., 2015b; Alonso et al., 2016; Tavernelli et al., 2019). We believe that these inclusion-body like structures are not occurring due to protein misfolding but as a consequence of the accumulation of ATAT-HA in a specific region of the cytoskeleton. Suggestively, we also observe an accumulation of acetylated α -tubulin around the kinetoplast and the inclusion body-like structure at the anterior region, where in normal conditions *Tc*ATAT is proposed to acetylate the microtubules as they polymerize. It is proposed that *T. cruzi* kinetoplast division is similar to that described to *Crithidia fasciculata* (Ferguson et al., 1994; Liu et al., 2005) and since the kinetoplast is part of the single mitochondrion, it is suggested that trypanosomatid's mitochondrion could start to segregate in the kinetoplast region (Ramos et al., 2011), which correlates with our observations. We propose that hyperacetylation impairs the division of the kDNA, given that the kinetoplast divides in coordination with the basal body. Cytoskeletal elements such as the flagellum, FAZ, flagellar pocket and the subpellicular microtubule array, all need to be duplicated and segregated in a coordinated manner in relation to the nuclear and kinetoplast cycles. The basal body in trypanosomes is the master organizer for the surrounding cytoskeleton, membranous structures, and organelles. Regulation of the basal body maturation, biogenesis, segregation and positioning is vital to ensure the shape and form of subsequent daughter cells (Elias et al., 2007). Further studies are required to determine the exact role of α -tubulin acetylation in the division of the kinetoplast and the basal body.

Oliveira Santos et al. described the effect of Trichostatin A (TSA), a deacetylase inhibitor in *T. cruzi*. They report that one of the main effects of TSA treatment is α -tubulin hyperacetylation, which induced microtubule cytoskeleton reorganization. They observed the presence of parasites with replicated kDNA, associated with basal bodies, but an incomplete cytokinesis. They also reported a higher number of protozoa in G2/M phase of the cell cycle and polynucleated cells with an aberrant phenotype (Santos et al., 2018). These results are similar to those observed in ATAT-HA over-expressing cells. Probably TSA treatment is targeting several deacetylases in *T. cruzi*, so it could promote the hyperacetylation of other proteins besides α -tubulin, but the cytoskeletal remodeling seems to be linked to α -tubulin acetylation.

Our study is the first report of the ATAT/MEC-17 homolog in trypanosomatids. Besides ATAT/MEC-17 itself, no other substrates than α -tubulin have been reported for this family of lysine acetyltransferases to date. Mammalian ATAT has been shown to localize to the lumen of MTs, where it exerts its KAT activity *in vitro* (Szyk et al., 2014). *Tc*ATAT-HA tight association with MTs could also be due to the same luminal localization but this needs further corroboration. Our results suggest that a precise amount of acetylated/non-acetylated α -tubulin is necessary for the correct kinetoplast division and assembly/disassembly of the basal body and the flagellum in epimastigotes. Further experiments are needed to determine the possible effect of α -tubulin hyperacetylation over the other stages of *T. cruzi* life cycle.

DATA AVAILABILITY STATEMENT

The raw data supporting the conclusions of this article will be made available by the authors, without undue reservation.

AUTHOR CONTRIBUTIONS

Conceived and designed the experiments: VA, MC, MM, CG, and ES. Performed the experiments: VA, MC, CG, GMP, MEC, AP, and LT. Wrote the manuscript: VA, MM, and ES. All authors contributed to the article and approved the submitted version.

FUNDING

This work was supported by Agencia Nacional de Promoción Científica y Tecnológica, Ministerio de Ciencia, Tecnología e Innovación Productiva, Argentina [PICT 2017–1978], Universidad Nacional de Rosario [PIP 1BIO490] and Research Council United Kingdom [MR/P027989/1] and also by Conselho

REFERENCES

- Akella, J. S., Wloga, D., Kim, J., Starostina, N. G., Lyons-Abbott, S., Morrisette, N. S., et al. (2010). MEC-17 is an α -tubulin acetyltransferase. *Nature* 467, 218–222. doi: 10.1038/nature09324
- Al-Bassam, J., and Corbett, K. D. (2012). α -Tubulin acetylation from the inside out. *Proc. Natl. Acad. Sci.* 109, 19515–19516. doi: 10.1073/pnas.1217594109
- Alonso, V. L., Ritagliati, C., Cribb, P., and Serra, E. C. (2014a). Construction of three new gateway[®] expression plasmids for *Trypanosoma cruzi*. *Mem. Inst. Oswaldo Cruz* 109, 1081–1085. doi: 10.1590/0074-0276140238
- Alonso, V. L., Villanova, G. V., Ritagliati, C., Motta, M. C. M., Cribb, P., and Serra, E. C. (2014b). *Trypanosoma cruzi* bromodomain factor 3 binds acetylated α -tubulin and concentrates in the flagellum during metacyclogenesis. *Eukaryot. Cell* 13, 822–831. doi: 10.1128/EC.00341-13
- Alonso, V. L., Ritagliati, C., Cribb, P., Cricco, J. A., and Serra, E. C. (2016). Overexpression of bromodomain factor 3 in *Trypanosoma cruzi* (TcBDF3) affects differentiation of the parasite and protects it against bromodomain inhibitors. *FEBS J.* 283, 2051–2066. doi: 10.1111/febs.13719
- Armson, A., Menon, K., O'Hara, A., MacDonald, L. M., Read, C. M., Sargent, K., et al. (2002). Efficacy of oryzalin and associated histological changes in *Cryptosporidium*-infected neonatal rats. *Parasitology* 125, 113–117. doi: 10.1017/s003118200200197x
- Bernhard, W. (1969). A new staining procedure for electron microscopical cytology. *J. Ultrastruct. Res.* 27, 250–265. doi: 10.1016/s0022-5320(69)80016-x
- Campos, P. C., Silva, V. G., Furtado, C., Machado-Silva, A., DaRocha, W. D., Peloso, E. F., et al. (2011). *Trypanosoma cruzi* MSH2: Functional analyses on different parasite strains provide evidences for a role on the oxidative stress response. *Mol. Biochem. Parasitol.* 176, 8–16. doi: 10.1016/j.molbiopara.2010.11.001
- Catta-Preta, C. M. C., Brum, F. L., da Silva, C. C., Zuma, A. A., Elias, M. C., de Souza, W., et al. (2015). Endosymbiosis in trypanosomatid protozoa: the bacterium division is controlled during the host cell cycle. *Front. Microbiol.* 6, 520. doi: 10.3389/fmicb.2015.00520
- Cavalcanti, D. P., Thiry, M., De Souza, W., and Motta, M. C. M. (2008). The kinetoplast ultrastructural organization of endosymbiont-bearing trypanosomatids as revealed by deep-etching, cytochemical and immunocytochemical analysis. *Histochem. Cell Biol.* 130, 1177–1185. doi: 10.1007/s00418-008-0450-7
- Chan, M. M. Y., Triemer, R. E., and Fong, D. (1991). Effect of the anti-microtubule drug oryzalin on growth and differentiation of the parasitic protozoan *Leishmania mexicana*. *Differentiation* 46, 15–21. doi: 10.1111/j.1432-0436.1991.tb00861.x

Nacional de Desenvolvimento Científico e Tecnológico (CNPq) and Fundação de Amparo à Pesquisa do Estado do Rio de Janeiro (FAPERJ).

ACKNOWLEDGMENTS

We would like to thank Rodrigo Vena, Dolores Campos, Romina Manarin, and Mara Ojeda for their technical assistance in confocal microscopy, cells and parasites culture and flow cytometry, respectively. Also, we are grateful to Carla Ritagliati for the assistance with motility measurements using the CASA Hamilton equipment.

SUPPLEMENTARY MATERIAL

The Supplementary Material for this article can be found online at: <https://www.frontiersin.org/articles/10.3389/fcimb.2021.642271/full#supplementary-material>

- Chung, C. G., Lee, H., and Lee, S. B. (2018). Mechanisms of protein toxicity in neurodegenerative diseases. *Cell. Mol. Life Sci.* 75, 3159–3180. doi: 10.1007/s00018-018-2854-4
- Coombes, C., Yamamoto, A., McClellan, M., Reid, T. A., Plooster, M., Luxton, G. W. G., et al. (2016). Mechanism of microtubule lumen entry for the α -tubulin acetyltransferase enzyme α TAT1. *Proc. Natl. Acad. Sci.* 113, E7176–E7184. doi: 10.1073/pnas.1605397113
- Cueva, J. G., Hsin, J., Huang, K. C., and Goodman, M. B. (2012). Posttranslational acetylation of α -tubulin constrains protofilament number in native microtubules. *Curr. Biol.* 22, 1066–1074. doi: 10.1016/j.cub.2012.05.012
- Deng, W., Wang, C., Zhang, Y., Xu, Y., Zhang, S., Liu, Z., et al. (2016). GPS-PAIL: prediction of lysine acetyltransferase-specific modification sites from protein sequences. *Sci. Rep.* 6:39787. doi: 10.1038/srep39787
- Dostál, V., and Libusová, L. (2014). Microtubule drugs: Action, selectivity, and resistance across the kingdoms of life. *Protozoa* 251, 991–1005. doi: 10.1007/s00709-014-0633-0
- Dyda, F., Klein, D. C., and Hickman, A. B. (2000). GCN5-related N-acetyltransferases: A structural overview. *Annu. Rev. Biophys. Biomol. Struct.* 29, 81–103. doi: 10.1146/annurev.biophys.29.1.81
- Elias, M. C., da Cunha, J. P. C., de Faria, F. P., Mortara, R. A., Freymüller, E., and Schenkman, S. (2007). Morphological Events during the *Trypanosoma cruzi* Cell Cycle. *Protist* 158, 147–157. doi: 10.1016/j.protis.2006.10.002
- Eshun-Wilson, L., Zhang, R., Portran, D., Nachury, M., Toso, D., Lohr, T., et al. (2019). Effects of α -tubulin acetylation on microtubule structure and stability. *Proc. Natl. Acad. Sci.* 116, 1–35. doi: 10.1073/pnas.1900441116
- Fassolari, M., and Alonso, G. D. (2019). Aurora kinase protein family in *Trypanosoma cruzi*: novel role of an AUK-B homologue in kinetoplast replication. *PLoS Negl. Trop. Dis.* 1–25.
- Ferguson, M. L., Torri, A. F., Pérez-Morga, D., Ward, D. C., and Englund, P. T. (1994). Kinetoplast DNA replication: mechanistic differences between *Trypanosoma brucei* and *Crithidia fasciculata*. *J. Cell Biol.* 126, 631–639. doi: 10.1083/jcb.126.3.631
- Gadadhar, S., Bodakuntla, S., Natarajan, K., and Janke, C. (2017). The tubulin code at a glance. *J. Cell Sci.* 130, 1347–1353. doi: 10.1242/jcs.199471
- Howes, S. C., Alushin, G. M., Shida, T., Nachury, M. V., and Nogales, E. (2013). Effects of tubulin acetylation and tubulin acetyltransferase binding on microtubule structure. *Mol. Biol. Cell* 25, 257–266. doi: 10.1091/mbc.e13-07-0387
- Hubbert, C., Guardiola, A., Shao, R., Kawaguchi, Y., Ito, A., Nixon, A., et al. (2002). HDAC6 is a microtubule-associated deacetylase. *Nature* 417, 455–458. doi: 10.1038/417455a

- Kalebic, N., Martinez, C., Perlas, E., Hublitz, P., Bilbao-Cortes, D., Fiedorczuk, K., et al. (2012). Tubulin Acetyltransferase α TAT1 Destabilizes Microtubules Independently of Its Acetylation Activity. *Mol. Cell. Biol.* 33, 1114–1123. doi: 10.1128/mcb.01044-12
- Kaser, S., Warscheid, B., Chanfon, A., Ochsenreiter, T., Pusnik, M., Meisinger, C., et al. (2014). Trypanosomal TAC40 constitutes a novel subclass of mitochondrial-barrel proteins specialized in mitochondrial genome inheritance. *Proc. Natl. Acad. Sci.* 111, 7624–7629. doi: 10.1073/pnas.1404854111
- Kim, G. W., Li, L., Ghorbani, M., You, L., and Yang, X. J. (2013). Mice lacking α -tubulin acetyltransferase 1 are viable but display α -tubulin acetylation deficiency and dentate gyrus distortion. *J. Biol. Chem.* 288 (28), 20334–20350. doi: 10.1074/jbc.M113.464792
- Kim, S. I., Kim, H. J., Lee, H. J., Lee, K., Hong, D., Lim, H., et al. (2016). Application of a non-hazardous vital dye for cell counting with automated cell counters. *Anal. Biochem.* 492, 8–12. doi: 10.1016/j.ab.2015.09.010
- Kull, F. J., and Sloboda, R. D. (2014). A slow dance for microtubule acetylation. *Cell* 157, 1255–1256. doi: 10.1016/j.cell.2014.05.021
- Li, L., Wei, D., Wang, Q., Pan, J., Liu, R., Zhang, X., et al. (2012). MEC-17 deficiency leads to reduced α -tubulin acetylation and impaired migration of cortical neurons. *J. Neurosci.* 32, 12673–12683. doi: 10.1523/JNEUROSCI.0016-12.2012
- Li, Y., Shah-Simpson, S., Okrah, K., Belew, A. T., Choi, J., Caradonna, K. L., et al. (2016). Transcriptome Remodeling in *Trypanosoma cruzi* and Human Cells during Intracellular Infection. *PLoS Pathog.* 12, e1005511. doi: 10.1371/journal.ppat.1005511
- Liu, B., Liu, Y., Motyka, S. A., Agbo, E. E. C., and Englund, P. T. (2005). Fellowship of the rings: the replication of kinetoplast DNA. *Trends Parasitol.* 21, 363–369. doi: 10.1016/j.pt.2005.06.008
- L'Hernault, S. W., and Rosenbaum, J. L. (1985). Chlamydomonas alpha-tubulin is posttranslationally modified by acetylation on the epsilon-amino group of a lysine. *Biochemistry* 24, 473–478. doi: 10.1021/bi00323a034
- Makioka, A., Kumagai, M., Ohtomo, H., Kobayashi, S., and Takeuchi, T. (2000). Effect of the antitubulin drug oryzalin on the encystation of *Entamoeba invadens*. *Parasitol. Res.* 86, 625–629. doi: 10.1007/pl00008542
- Morejohn, L. C., Bureau, T. E., Molè-Bajer, J., Bajer, A. S., and Fosket, D. E. (1987). Oryzalin, a dinitroaniline herbicide, binds to plant tubulin and inhibits microtubule polymerization in vitro. *Planta* 172, 252–264. doi: 10.1007/BF00394595
- Moretti, N. S., Cestari, I., Anupama, A., Stuart, K., and Schenkman, S. (2018). Comparative Proteomic Analysis of Lysine Acetylation in *Trypanosomes*. *J. Proteome Res.* 17, 374–385. doi: 10.1021/acs.jproteome.7b00603
- Nakakura, T., Asano-Hoshino, A., Suzuki, T., Arisawa, K., Tanaka, H., Sekino, Y., et al. (2015). The elongation of primary cilia via the acetylation of α -tubulin by the treatment with lithium chloride in human fibroblast KD cells. *Med. Mol. Morphol.* 48, 44–53. doi: 10.1007/s00795-014-0076-x
- Nett, I. R. E., Martin, D. M. A., Miranda-Saavedra, D., Lamont, D., Barber, J. D., Mehlert, A., et al. (2009). The phosphoproteome of bloodstream form *Trypanosoma brucei*, causative agent of African sleeping sickness. *Mol. Cell. Proteomics* 8, 1527–1538. doi: 10.1074/mcp.M800556-MCP200
- Piperno, G., LeDizet, M., and Chang, X. J. (1987). Microtubules containing acetylated alpha-tubulin in mammalian cells in culture. *J. Cell Biol.* 104, 289–302. doi: 10.1083/jcb.104.2.289
- Portran, D., Schaedel, L., Xu, Z., Théry, M., and Nachury, M. V. (2017). Tubulin acetylation protects long-lived microtubules against mechanical ageing. *Nat. Cell Biol.* 19, 391–398. doi: 10.1038/ncb3481
- Price, H. P., Peltan, A., Stark, M., and Smith, D. F. (2010). The small GTPase ARL2 is required for cytokinesis in *Trypanosoma brucei*. *Mol. Biochem. Parasitol.* 173, 123–131. doi: 10.1016/j.molbiopara.2010.05.016
- Ramos, T. C. P., Freymüller-Haapalainen, E., and Schenkman, S. (2011). Three-dimensional reconstruction of *Trypanosoma cruzi* epimastigotes and organelle distribution along the cell division cycle. *Cytometry A.* 79 (7), 538–544. doi: 10.1002/cyto.a.21077
- Ritagliati, C., Alonso, V. L., Manarin, R., Cribb, P., and Serra, E. C. (2015a). Overexpression of Cytoplasmic TcSIR2RP1 and Mitochondrial TcSIR2RP3 Impacts on *Trypanosoma cruzi* Growth and Cell Invasion. *PLoS Negl. Trop. Dis.* 9, 1–22. doi: 10.1371/journal.pntd.0003725
- Ritagliati, C., Villanova, G. V., Alonso, V. L., Zuma, A., Cribb, P., Motta, M. C. M., et al. (2015b). Glycosomal bromodomain factor 1 from *Trypanosoma cruzi* enhances trypanomastigote cell infection and intracellular amastigote growth. *Biochem. J.* 473, 73–85. doi: 10.1042/bj20150986
- Rosenzweig, D., Smith, D., Myler, P. J., Olafson, R. W., and Zilberstein, D. (2008). Post-translational modification of cellular proteins during *Leishmania donovani* differentiation. *Proteomics* 8, 1843–1850. doi: 10.1002/pmic.200701043
- Saborio, J. L., Manuel Hernandez, J., Narayanswami, S., Wrightsman, R., Palmer, E., Manning, J., et al. (1989). Isolation and Characterization of Paraflagellar Proteins from *Trypanosoma cruzi*. *J. Biol. Chem.* 264, 4071–4075. doi: 10.1016/S0021-9258(19)84963-3
- Sanchez, A. D., and Feldman, J. L. (2017). Microtubule-organizing centers: from the centrosome to non-centrosomal sites. *Curr. Opin. Cell Biol.* 44, 93–101. doi: 10.1016/j.cceb.2016.09.003
- Santos, d., Zuma, A. A., Francisca, N., da Cunha, J. P. C., de Souza, W., and Motta, M. C. M. (2018). Trichostatin A induces *Trypanosoma cruzi* histone and tubulin acetylation: effects on cell division and microtubule cytoskeleton remodelling. *Parasitology* 146 (4), 543–552. doi: 10.1017/S0031182018001828
- Sasse, R., and Gull, K. (1988). Tubulin post-translational modifications and the construction of microtubular organelles in *Trypanosoma brucei*. *J. Cell Sci.* 90 (Pt 4), 577–589.
- Schindelin, J., Arganda-Carreras, I., Frise, E., Kaynig, V., Longair, M., Pietzsch, T., et al. (2012). Fiji: an open-source platform for biological-image analysis. *Nat Methods* 9 (7), 676–682. doi: 10.1038/nmeth.2019
- Schneider, A., Sherwin, T., Sasse, R., Russell, D. G., Gull, K., and Seebeck, T. (1987). Subpellicular and Flagellar Microtubules of *Trypanosoma brucei* brucei Contain the Same α -Tubulin Isoforms. *J. Cell Biol.* 104, 431–438. doi: 10.1083/jcb.104.3.431
- Shaw, M. K., Compton, H. L., Roos, D. S., and Tilney, L. G. (2000). Microtubules, but not actin filaments, drive daughter cell budding and cell division in *Toxoplasma gondii*. *J. Cell Sci.* 113, 1241 LP–1254.
- Shida, T., Cueva, J. G., Xu, Z., Goodman, M. B., and Nachury, M. V. (2010). The major α -tubulin K40 acetyltransferase TAT1 promotes rapid ciliogenesis and efficient mechanosensation. *Proc. Natl. Acad. Sci.* 107, 21517–21522. doi: 10.1073/pnas.1013728107
- Singh, S., and Panda, A. K. (2005). Solubilization and refolding of bacterial inclusion body proteins. *J. Biosci. Bioeng.* 99 4, 303–310. doi: 10.1263/jbb.99.303
- Smircich, P., Eastman, G., Bispo, S., Duhagon, M. A., Guerra-Slompo, E. P., Garat, B., et al. (2015). Ribosome profiling reveals translation control as a key mechanism generating differential gene expression in *Trypanosoma cruzi*. *BMC Genomics* 16, 443. doi: 10.1186/s12864-015-1563-8
- Souto-Padron, T., Cunha e Silva, N. L., and de Souza, W. (1993). Acetylated alpha-tubulin in *Trypanosoma cruzi*: immunocytochemical localization. *Mem. Inst. Oswaldo Cruz* 88, 517–528. doi: 10.1590/S0074-02761993000400004
- Stargell, L. A., Heruth, D. P., Gaertig, J., and Gorovsky, M. A. (1992). Drugs affecting microtubule dynamics increase alpha-tubulin mRNA accumulation via transcription in *Tetrahymena thermophila*. *Mol. Cell. Biol.* 12, 1443–1450. doi: 10.1128/mcb.12.4.1443
- Stokkermans, T. J. W., Schwartzman, J. D., Keenan, K., Morrissette, N. S., Tilney, L. G., and Roos, D. S. (1996). Inhibition of *Toxoplasma gondii* replication by dinitroaniline herbicides. *Exp. Parasitol.* 84, 355–370. doi: 10.1006/expr.1996.0124
- Szyk, A., Deaconescu, A. M., Spector, J., Goodman, B., Valenstein, M. L., Ziolkowska, N. E., et al. (2014). Molecular basis for age-dependent microtubule acetylation by tubulin acetyltransferase. *Cell* 157, 1405–1415. doi: 10.1016/j.cell.2014.03.061
- Tavernelli, L. E., Motta, M. C. M., Gonçalves, C. S., da Silva, M. S., Elias, M. C., Alonso, V. L., et al. (2019). Overexpression of *Trypanosoma cruzi* High Mobility Group B protein (TcHMGB) alters the nuclear structure, impairs cytokinesis and reduces the parasite infectivity. *Sci. Rep.* 9, 1–16. doi: 10.1038/s41598-018-36718-0
- Taylor, M. C., and Kelly, J. M. (2006). pTcINDEX: A stable tetracycline-regulated expression vector for *Trypanosoma cruzi*. *BMC Biotechnol.* 6, 1–18. doi: 10.1186/1472-6750-6-32
- Traub-Cseko, Y. M., Ramalho-Ortigão, J. M., Dantas, A. P., de Castro, S. L., Barbosa, H. S., and Downing, K. H. (2002). Dinitroaniline herbicides against protozoan parasites: the case of *Trypanosoma cruzi*. *Trends Parasitol.* 17, 136–141. doi: 10.1016/S1471-4922(00)01834-1

- Tsigankov, P., Gherardini, P. F., Helmer-Citterich, M., Späth, G. F., and Zilberstein, D. (2013). Phosphoproteomic analysis of differentiating Leishmania parasites reveals a unique stage-specific phosphorylation motif. *J. Proteome Res.* 12, 3405–3412. doi: 10.1021/pr4002492
- Varberg, J. M., Padgett, L. R., Arrizabalaga, G., and Sullivan, W. J. (2015). TgATAT-Mediated alpha-Tubulin Acetylation Is Required for Division of the Protozoan Parasite *Toxoplasma gondii*. *mSphere* 1, 1–16. doi: 10.1128/mSphere.00088-15. Editor
- Vidal, J. C., Souza, W., de Vidal Cunha, J., and de Souza, W. (2017). Morphological and Functional Aspects of Cytoskeleton of Trypanosomatids. *Cytoskelet. - Struct. Dyn. Dis.* 55–72. doi: 10.5772/57353
- Wheeler, R. J., Gull, K., and Sunter, J. D. (2019). Coordination of the Cell Cycle in Trypanosomes. *Annu. Rev. Microbiol.* 73, 133–154. doi: 10.1146/annurev-micro-020518-115617
- World Health Organization (2012). Research priorities for Chagas disease, human African trypanosomiasis and leishmaniasis. *World Health Organ. Tech. Rep. Ser.* 975, v–xii, 1–100.
- Zhou, Q., and Li, Z. (2015). The γ -tubulin complex in *Trypanosoma brucei*: molecular composition, subunit interdependence and requirement for axonemal central pair protein assembly. *Mol. Microbiol.* 98, 667–680. doi: 10.1007/s11065-015-9294-9. Functional
- Zhou, H., Cheng, X., Xu, X., Jiang, T., Zhou, H., Sheng, Q., et al. (2018). Cloning, expression profiling, and acetylation identification of alpha-tubulin N-acetyltransferase 1 from *Bombyx mori*. *Arch. Insect Biochem. Physiol.* 98, 1–10. doi: 10.1002/arch.21463

Conflict of Interest: The authors declare that the research was conducted in the absence of any commercial or financial relationships that could be construed as a potential conflict of interest.

Copyright © 2021 Alonso, Carloni, Gonçalves, Martinez Peralta, Chesta, Pezza, Tavernelli, Motta and Serra. This is an open-access article distributed under the terms of the Creative Commons Attribution License (CC BY). The use, distribution or reproduction in other forums is permitted, provided the original author(s) and the copyright owner(s) are credited and that the original publication in this journal is cited, in accordance with accepted academic practice. No use, distribution or reproduction is permitted which does not comply with these terms.